THE JOURNAL OF PHYSICAL CHEMISTRY B

ARTICLE

pubs.acs.org/JPCB

Microscopic Structure and Dynamics of $LiBF_4$ Solutions in Cyclic and Linear Carbonates

O. O. Postupna,[†,‡] Y. V. Kolesnik,[†] O. N. Kalugin,[†] and O. V. Prezhdo[‡,*]

[†]Department of Inorganic Chemistry, V. N. Karazin Kharkiv National University, 61022, 4 Svoboda sq., Kharkiv, Ukraine

[‡]Department of Chemistry, University of Rochester, Rochester, New York 14627, United States

ABSTRACT: Motivated by development of lithium-ion batteries, we study the structure and dynamics of $LiBF_4$ in pure and mixed solvents with various salt concentrations. For this purpose, we have developed force field models for ethylene carbonate, propylene carbonate, dimethyl carbonate, and dimethoxyethane. We find that Li^+ is preferentially solvated by the cyclic and more polar component of the mixtures, as the electrostatic interaction overcomes possible steric hindrances. The cation coordination number decreases from 6 to 5 with increasing salt concentration due to formation of ion-pairs. The uniform decline of the diffusion coefficients of the two ions is disrupted at mixture compositions that perturb the ion-pair interaction. We show that the Stokes' model of diffusion can be applied to the very small Li^+ ion, provided that the size of the first solvation shell is properly taken into consideration. The strong coordination of the ions by the polar, cyclic components of the solvent mixtures established in our simulations suggests that the less polar linear component can be optimized in order to reduce electrolyte viscosity and to achieve high electrical conductivity.

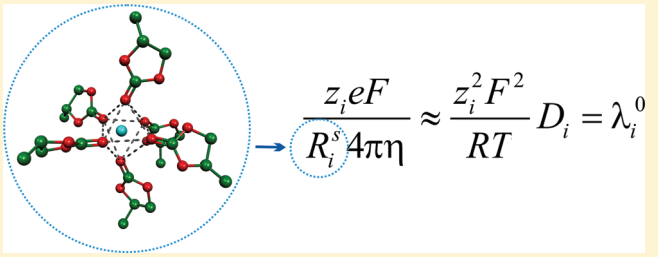

1. INTRODUCTION

Electrolyte solutions of lithium salts in mixed organic solvents are of great importance for the development of lithium-ion batteries. Solvents that exhibit wide electrochemical windows are particularly important in battery applications, and aprotic solvents provide a broad range of possibilities in this regard.[1−4] A compromise between high electrical conductivity and low viscosity can be achieved by mixtures of highly polar cyclic ethers, such as ethylene carbonate (EC) and propylene carbonate (PC), with linear ethers, such as dimethoxyethane (DME), dimethyl carbonate (DMC), diethyl carbonate and ethylmethyl carbonate.[1,5−11] Lithium tetrafluoroborates and perchlorates are among the most actively used electrolytes.[12,13]

EC (1,3-dioxolane-2-one, $C_3H_4O_3$) and PC (4-methyl-1, 3-dioxolan-2-one, $C_4H_6O_3$, Figure 1) are polar aprotic solvents. The high dielectric permittivity ε values of these solvents (89.78 and 64.92, respectively) constitute an indisputable merit from the electrochemical point of view. At the same time, EC and PC exhibit high viscosity η (1.90 and 2.53 mPa·s, respectively), which is a major drawback in battery applications. DMC ($C_3H_6O_3$) and DME (1,2-dimethoxyethane, $C_4H_{10}O_2$, Figure 1) are linear ethers with high electrochemical stability and low viscosity (0.59 and 0.41 mPa·s, respectively). At the same time, they have low dielectric constants (3.11 and 7.03, respectively).

EC−DMC and PC−DME mixtures are used in Li-ion electrochemical cells. More generally, salt solutions in these mixtures can be viewed as model systems for investigation of physical and chemical properties of 1−1 electrolyte solutions.[14]

The complexity of experiments and data interpretation hinders development of a comprehensive molecular understanding of the factors that determine the key properties of electrolytes used in Li-ion batteries.[15,16] The microscopic descriptions found in literature vary significantly with experimental technique, and approximations made in the data analysis. For example, there exists no consensus on the structure of the first solvation shell of the lithium ion, and the Li^+ coordination number remains generally unknown. Various authors report coordination numbers anywhere between 2 and 8.[17−22] Such state of affairs creates strong motivation for molecular dynamics (MD) simulations, which are capable of providing an atomistic description of both microscopic and macroscopic characteristics of electrolyte systems. For instance, MD simulations can generate convincing evidence regarding the Li^+ ion solvation structure, which carries a strong impact on the electrical conductivity of solutions.

All-atom polarizable molecular models of EC, PC, DMC, DME, and similar substances are widely used in MD simulations.[8−10] Such advanced models are particularly appropriate for precise calculation of the vibrational spectra of these molecules. At the same time, a detailed representation of all internal degrees of freedom significantly raises the computational effort compared to simpler models, while the benefits of such representation for the simulation of ion solvation and diffusion are not immediately clear. Soetens et al. proposed all-atom polarizable models for the EC, PC, and DMC molecules.[23] The MD simulation of EC was performed at temperatures above 50 °C. A racemic mixture of enantiomers was simulated for PC. The dipole moments were slightly overestimated, while the diffusion coefficients were accurate. The MD simulations on liquid PC reported by Borodin

Received: June 26, 2011
Revised: October 11, 2011
Published: October 13, 2011

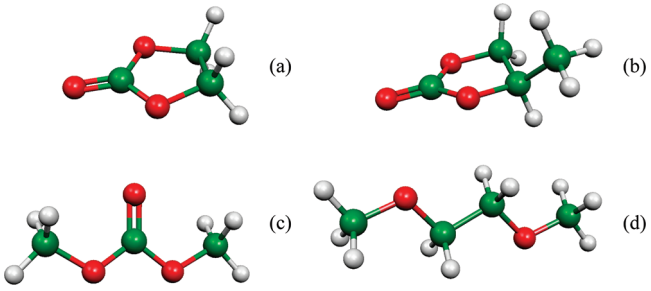

Figure 1. Molecular structure of (a) EC, (b) PC, (c) DMC, and (d) DME.

and Smith provided adequate values for the electrical conductivity, but not for the diffusion coefficient.[9]

Vorobyov et al.[10] used an all-atom polarizable model of DME and obtained good thermodynamic properties, while underestimating the dielectric permittivity. Borodin and Smith carried out MD simulation using an all-atom polarizable model and reported good agreement with the experimental values for density and electrical conductivity, while observing large deviations for the diffusion coefficients, on the order of 40%.[9]

The variety of atomistic models developed for these substances highlights the main problem: there exists no universal representation, even at the rather sophisticated level of description, which is able to describe simultaneously and adequately all important characteristics. Each model is applicable only for investigation of a rather narrow set of properties. Moreover, the reports available in the literature focus on pure substances, whereas development of Li-ion batteries requires modeling of solvent mixtures over a broad range of compositions, as well as of electrolyte solutions in such mixtures.

This paper aims to determine the influence of the solvent properties and electrolyte concentration on the structural and dynamic characteristics of lithium tetrafluoroborate solutions in mixtures of EC, PC, DMC, and DME. Particular attention is given to the structure of the first solvation shell (FSS) of the Li^+ ion in these mixed solvents. Molecular understanding of the FSS structure makes it possible to rationalize the behavior of the electrical conductivity and ion diffusion coefficients as a function of solvent composition, electrolyte concentration and other variables and to predict these characteristics for analogous systems.

The molecular models chosen in this work seek to combine both practical and fundamental aspects of the simulation. In this case, a model should be applicable to investigation of structural and dynamic properties of $LiBF_4$ solutions in EC, PC, DMC, and DME, in mixed solvents, and at different salt concentration. Only a comprehensive investigation of this kind can provide the desired atomistic interpretation of the experimental data, as well as adequately predict various physical and chemical properties for systems of this kind. In particular, we are able to establish which mixture component is responsible for solvating the ions and why and to investigate how salt concentration affects the ion coordination number. We study the effect of the $Li^+BF_4^-$ ion pair formation and its disruption by interaction with the solvent on solvation structure and ion diffusion rates. Further, we test the Stokes' model that provides the simplest description of ion diffusion, but that is not expected to work with small ions, such as Li^+. The conclusions drawn in this work generate a molecular level understanding of electrolyte properties and provide guidelines for optimization of electrolytes used in lithium-ion batteries.

The following section develops the force field models for the solvents and electrolyte. Comparison of MD results with the relevant experimental data justifies the validity of these models. Section three provides the technical details of the MD simulations, and specifies the investigated systems and their physical and chemical properties. The Results and Discussion section is split into two subsections devoted, respectively, to the structural and dynamical characteristics of the electrolyte solutions. The paper concludes with a summary of the key results, including a brief discussion of their relevance to the design of Li-ion batteries.[15,16]

2. DEVELOPMENT AND VALIDATION OF FORCE FIELD MODELS

In the present work, the system's potential energy U was calculated as a sum of the intermolecular U^{inter} and intramolecular U^{intra} interaction energies

$$U = U^{inter} + U^{intra} \tag{1}$$

The intermolecular interactions were represented with the long-range (Coulomb) U^{Coul} and short-range (Lennard-Jones) U^{LJ} interaction potentials

$$U^{inter} = U^{Coul} + U^{LJ} \tag{2}$$

In order to take into account electrostatic interactions, the reaction field method was applied. According to this method, pair Coulomb potentials are calculated as follows:

$$U_{ij}^{Coul}(r) = \frac{z_i z_j e^2}{4\pi\varepsilon_0}\left[\frac{1}{r} - \frac{1}{R_c} + \frac{\varepsilon - 1}{2\varepsilon + 1}\left(\frac{r^2}{R_c{}^3} - \frac{1}{R_c}\right)\right] \tag{3}$$

where r is the distance between the charges, z_i and z_j are the partial charges on atoms i and j, respectively, ε is the effective dielectric permittivity of a simulated system, and R_c is the cutoff radius. Short-range interactions were calculated using the Lennard-Jones 12−6 shifted force potential; the ε_{ij} and σ_{ij} parameters were calculated by applying the Lorentz−Berthelot combining rules.

The intramolecular interaction potential takes into account the energies associated with fluctuations of torsion angles ($U^{dihedral}$), and the energy of nonbonded interactions (U^{NB}) between atoms separated by more than 3 bonds

$$U^{intra} = U^{NB} + U^{dihedral} \tag{4}$$

The nonbonded interaction potential was calculated similarly to the intermolecular interaction potential by eq 2. The equilibrium values of bond lengths and angles for rigid molecular models of PC and EC were obtained through quantum chemical calculations. For flexible models, the intramolecular potentials are set explicitly as described below.

A molecular model should be designed to reproduce experimental values of physical and chemical properties of the simulated system. Additionally, it should be sufficiently simple in order to ensure computational efficiency. The latter depends strongly on the number of degrees of freedom in the system. Since fluctuations of bond lengths and valence angles have little effect on intermolecular interactions due to small amplitudes and high frequencies of the vibrations, fixed equilibrium bond lengths and angles were used. In contrast, changes in torsion angles lead

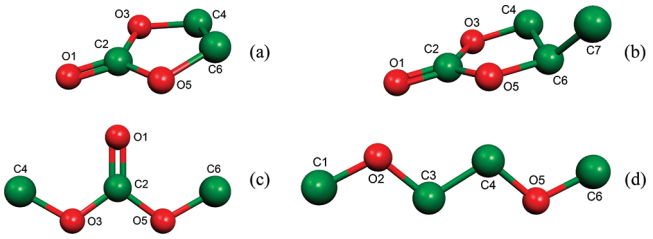

Figure 2. Molecular dynamics models of (a) EC, (b) PC, (c) DMC, and (d) DME.

to significant atomic displacements and notably modify molecular conformations. Consequently, in order to minimize the number of degrees of freedom of the system, we considered explicitly only the functional dependence of the potential on torsion angles. Its analytical form, U^{dihedral}, was represented with the Ryckaert–Bellmans potential[24]

$$U_{\text{RB}}^{\text{dihedral}}(\beta_{ijkl}) = \sum_n c_n \cos^n \beta_{ijkl} \quad (5)$$

where β_{ijkl} is the equilibrium value of the torsion angle, and c_n are parameters. Note that the dihedral angle β_{ijkl} equals to 180 degrees for trans-configurations.

The molecular geometries were optimized using the Onsager reaction field model at the B3LYP/cc-pVTZ level of theory in the GAUSSIAN 03 quantum chemical package.[25] The dielectric constants of the media were set equal to that of the pure solvents. The partial atomic charges were calculated using the Breneman ChelpG method[26] at the B3LYP/aug-cc-pVTZ level of theory including the medium effects.

In order to reduce the MD simulation time, a united atom representation of the CH, CH_2, and CH_3 groups was used (compare Figures 1 and 2). This simplification had little effect on the properties investigated below, because the united atom Lennard-Jones parameters properly represent the relevant inter- and intramolecular interactions.

In order to define an analytical form of the $U_i(\beta)$ potential for DME, a series of quantum chemical calculations (QCC) were carried out for the DME molecule with different values of the dihedral angles $\beta_{O2-C3-C4-O5}$ and $\beta_{C1-O2-C3-C4}$. The dihedral angle $\beta_{C3-C4-O5-C6}$ was set equal to 180°. The B3LYP/6-31G(d) level of theory was used. The dihedral parameters were calculated using the weighted method of least-squares, thereby optimizing the many-body contributions to the potential. The parameters for $\beta_{C1-O2-C3-C4}$ and $\beta_{C3-C4-O5-C6}$ were assumed equal. The DME conformation with the dihedral angles $\beta_{O2-C3-C4-O5} = \beta_{C1-O2-C3-C4} = 180°$ is the most stable according to the QCC (Figure 2d). Its energy is more than 4 kJ/mol lower than that of the other hindered conformations (Figure 3). The same procedure was applied for deriving the intramoleculer potential of DMC (Table 1).

In order to obtain the atomic charges for the DME molecule, all 27 hindered conformations were divided by symmetry into 10 groups. Confirmations within each group could be transformed from one to another using reflection operations and permutations of atom numbers. The partial atomic charges at all 16 atoms of the DME molecule were calculated for the 27 conformations.

The parameters used in the MD simulations are given in Table 1. The Lennard-Jones parameters for all interaction sites were taken from the GROMOS 96 force field model,[27] except for σ_{ii} and ε_{ii} for the C2 atom of carbonates, which were set equal to

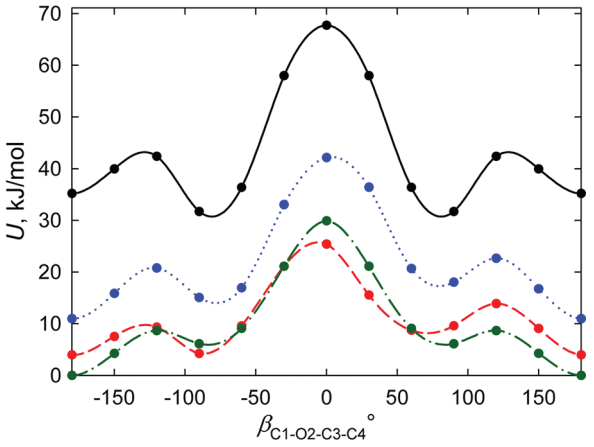

Figure 3. Dependence of the internal energy of the DME molecule on conformation. The black solid, red dashed, blue dotted, and green dash-dotted lines correspond to the following fixed values of the O2–C3–C4–O5 torsional angle, respectively (Figure 2): 0, 60, 120, and 180°.

0.41 nm and 0.05 kJ/mol, respectively. The QCC charges were reduced by 5% for EC and 10% for PC, significantly improving agreement with the experimental data for heat of vaporization ($\Delta_{\text{vap}}H^0_{298}$), viscosity ($\eta$), and dielectric permittivity (ε; Table 2). The calculations were carried out for one of the two possible PC molecular isomers, since it was found that the pure L-isomer and the racemic mixture of L- and D-isomers possess almost identical physical and chemical properties.

The geometry and partial atomic charges for the BF_4^- ion atoms were calculated in vacuum at the B3LYP/aug-cc-pVTZ level of theory. The ion's Lennard-Jones parameters were taken from ref 22.

The Lennard-Jones 12–6 potential parameters for Li^+ were recalculated from the van der Waals parameters given in ref 28 preserving the depth and location of the Li–Li distance potential energy minimum.

In order to validate the developed force fields, the MD simulation results were compared to the experimental data[29] on some macroscopic properties ($\Delta_{\text{vap}}H^0_{298}$, η, ε) of pure solvents. As seen in Table 2, the developed models adequately describe these properties, and consequently, they can be applied reliably to further MD simulation.

3. MD SIMULATION DETAILS

In order to investigate the structural and dynamic properties of the $LiBF_4$ solutions in PC–DME and EC–DMC MD simulations were carried out for the following systems: pure EC, PC, DMC, and DME; the PC–DME mixtures with the PC molar fraction of 25%, 50%, and 75%; the EC–DMC mixture with EC molar fraction of 50%; infinitely diluted Li^+ and BF_4^- solutions in pure solvents and their mixtures; $Li^+BF_4^-$ ion pairs in DME and $LiBF_4$ in the EC–DMC mixtures; solutions with $LiBF_4$ concentration of approximately 0.1 mol·dm^{-3} in PC, PC–DME, and EC–DMC; and solutions with $LiBF_4$ concentration of approximately 1.0 mol·dm^{-3} in pure PC, PC–DME, and EC–DMC. A detailed list of all systems can be found in Tables 3 and 4 together with MD simulation details.

The dielectric constants of the mixtures were calculated from the experimental data.[30,31] The densities of the PC–DME and EC–DMC solutions, the 0.1 and 1.0 mol·dm^{-3} $LiBF_4$ solutions

Table 1. Force Field Parameters for the EC, PC, DMC, and DME Molecules

ethylene carbonate			
interaction center	q, $\|e\|$	σ_{ii}, nm	ε_{ii}, kJ/mol
O1	−0.59531	0.296	0.87864
C2	0.86885	0.41	0.05
O3	−0.43160	0.300	0.71128
C4	0.29483	0.350	0.276144
O5	−0.43160	0.300	0.71128
C6	0.29483	0.350	0.276144
propylene carbonate			
interaction center	q, $\|e\|$	σ_{ii}, nm	ε_{ii}, kJ/mol
O1	−0.55981	0.263	1.724
C2	0.83925	0.41	0.05
O3	−0.31931	0.295	0.850
C4	0.12917	0.392	0.490
O5	−0.51437	0.295	0.850
C6	0.32981	0.314	0.380
C7	0.09526	0.383	0.732
dimethyl carbonate			
interaction center	q, $\|e\|$	σ_{ii}, nm	ε_{ii}, kJ/mol
O1	−0.5686	0.263	1.724
C2	0.9458	0.41	0.05
O3	−0.4326	0.295	0.850
C4	0.2440	0.383	0.732
$\angle$(C4−O3−C2) = 114.50°, $\angle$(O3−C2−O1) = 126.05°, $\angle$(O3−C2−O5) = 107.90°, r(C4−O3) = 0.1435 nm, r(O3−C2) = 0.1342 nm, r(C2−O1) = 0.1212 nm			
n		c_n for $U_1(\beta_{O1-C2-O3-C4})$, $U_2(\beta_{O3-C2-O5-C6})$, kJ/mol	
1		41.583	
2		−6.0702	
3		−35.211	
dimethoxyethane			
interaction center	q, $\|e\|$	σ_{ii}, nm	ε_{ii}, kJ/mol
C1	0.1813	0.383	0.732
O2	−0.3839	0.295	0.850
C3	0.2026	0.392	0.490
$\angle$(C3−O1−C2)= 113.01°, $\angle$(O1−C2−C3) = 107.80°, r(C3−O1) = 0.1410 nm, r(O1−C2) = 0.1412 nm, r(C2−C4) = 0.1516 nm			
n	c_n for $U_1(\beta_{C1-O2-C3-C4})$, $U_3(\beta_{C3-C4-O5-C6})$, kJ/mol	c_n for $U_2(\beta_{O2-C3-C4-O5})$, kJ/mol	
1	0.000	14.480	
2	−4.945	12.440	
3	11.260	12.800	
4	21.840	38.260	
5	−4.134	−3.967	
6	−3.235	−9.048	

Table 2. Comparison between MD Simulation and Experimental Data

	$\Delta_{vap}H^0_{298}$, kJ/mol		η, mPa·s		ε	
system	MD	exp	MD	exp	MD	exp
EC	55.53 ± 0.01	50.10	1.6 ± 0.3	1.93	161 ± 11	89.78
PC	67.11 ± 0.03	65.28	2.9 ± 0.4	2.53	59 ± 6	64.92
DMC	22.49 ± 0.03	37.26	0.62 ± 0.07	0.585	2	3.17
DME	36.76 ± 0.02	32.10	0.36 ± 0.03	0.455	7 ± 1	7.2

in pure PC and DME, and their mixtures were obtained from the experimental data.[7,30,31]

The simulations were carried out using the MDNAES program package[32] in the NVT ensemble at the temperature of 298.15 K, except for the EC solution, which was simulated at 313.15 K. The Berendsen thermostat[31] was applied to maintain constant temperature. The MD time step was equal to 0.002 ps, and the thermostat parameter was 0.5 ps. Each system was equilibrated for 1 ns (30 ns for concentrated solutions). The properties of interest were obtained by averaging over six production runs for each system. Each run was 2 ns long. In order to establish the convergence of the simulation results with respect to the simulation length, additional longer trajectories were obtained for some systems, as indicated in parentheses in Table 3.

4. RESULTS AND DISCUSSION

4.1. Structural Properties. The structure of the first coordination sphere of Li^+ ions in infinitely diluted solutions in the PC−DME and EC−DMC mixtures is characterized by the radial distribution functions (RDFs) (Figures 4 and 5). Analysis shows that that the FSS is determined by interaction of Li^+ with the oxygen atoms of the solvent molecules. In the case of the PC, EC, and DMC molecules, the oxygens of the carbonyl groups play a more important role than the oxygens imbedded in the hydrocarbon chain. A solvent molecule was considered to be part of the ion's FSS, if the lithium−oxygen distance remained less or equal to the location of the first minimum in corresponding RDF (0.36 nm for PC and 0.35 nm for EC, Figures 4 and 5).

The MD simulation for Li^+ in pure PC showed that the Li^+ FSS consisted of six molecules. Occasionally, as indicated by the running coordination number (RCN), only 5 molecules were seen in the Li^+ FSS. The simulation results appear in contrast with the spectroscopic data, according to which the Li^+ FSS may contain up to 4 PC molecules. However, it has been found[17] that spectroscopic methods (IR spectroscopy) tend to underestimate RCN for Li^+ solvated by PC. Reference 18 suggested that RCN is equal to 6.2 in this system. However, ref 19 questioned this value due to impossibility to arrange such a large number of PC molecules in the Li^+ FSS, given the molecule's size. We found that 6 PC molecules can be easily placed in the Li^+ FSS without any steric difficulties (Figure 6). It is important to note here that the σ_{ii} parameters of the Lennard-Jones potential, reflecting the effective atomic sizes for the solvent molecules in the MD simulation, correctly reproduce the equilibrium geometries and effective molecular volumes, and therefore, properly describe the FSS.

The authors of ref 17 used neutron scattering[33] with the $^6Li/^7Li$ substitution to characterize the solvation structure of Li^+ in 10 mol % $LiPF_6$−PC solutions. The measured RCN value

Table 3. Simulated Systems Containing PC and DME

		no. of solvent molecules						
no.	electrolyte	PC	DME	length of run	c, mol·dm^{-3}	m, mol·kg^{-1}	ρ, kg·m^{-3}	ε
1			216	6 × 2 ns			861.09	7.03
2		54	162	6 × 2 ns			940.37	19.77
3		108	108	6 × 2 ns			1023.02	33.68
4		162	54	6 × 2 ns			1109.44	48.74
5		216		6 × 2 ns			1198.00	64.92
6	1 Li^+		215	6 × 2 ns	0.00	0.00	861.09	7.03
7	1 Li^+	53	159	6 × 2 ns	0.00	0.00	940.37	19.77
8	1 Li^+	107	107	6 × 2 ns	0.00	0.00	1023.02	33.68
9	1 Li^+	159	53	6 × 2 ns	0.00	0.00	1109.44	48.74
10	1 Li^+	215		6 × 2 ns	0.00	0.00	1198.00	64.92
11	1 BF_4^-		215	6 × 2 ns	0.00	0.00	861.09	7.03
12	1 BF_4^-	53	159	6 × 2 ns	0.00	0.00	940.37	19.77
13	1 BF_4^-	107	107	6 × 2 ns	0.00	0.00	1023.02	33.68
14	1 BF_4^-	159	53	6 × 2 ns	0.00	0.00	1109.44	48.74
15	1 BF_4^-	215		6 × 2 ns	0.00	0.00	1198.00	64.92
16	1 $Li^+BF_4^-$		214	6 × 2 ns	0.00	0.00	865.70	7.03
17	2 $LiBF_4$	53	159	6 × 2 ns (12 × 2 ns)	0.0975	0.1013	1204.95	19.77
18	2 $LiBF_4$	106	106	6 × 2 ns (12 × 2 ns)	0.1025	0.0982	1045.30	33.68
19	2 $LiBF_4$	159	53	6 × 2 ns (18 × 2 ns)	0.1077	0.0952	1132.00	48.74
20	2 $LiBF_4$	212		6 × 1 ns (20 × 2 ns)	0.1113	0.0924	1204.95	64.92
21	16 $LiBF_4$	43	129	6 × 2 ns (20 × 2 ns)	1.0242	0.9990	1025.21	19.77
22	17 $LiBF_4$	88	88	6 × 2 ns (100 × 2 ns)	1.1151	1.0051	1127.90	33.68
23	18 $LiBF_4$	135	45	6 × 2 ns (50 × 2 ns)	1.1896	1.0091	1189.55	48.74
24	18 $LiBF_4$	176		6 × 2 ns (40 × 2 ns)	1.2574	1.0018	1255.18	64.92
25	144 $LiBF_4$	1408		(9 × 2 ns)	1.2574	1.0018	1255.18	64.92

Table 4. Simulated Systems Containing EC and DMC

no.	electrolyte	no. of EC molecules	no. of DMC molecules	c, mol·dm^{-3}	m, mol·kg^{-1}	ρ, kg·m^{-3}	ε
1			216			1063.0	3.10
2		108	108			1200.5	46.60
3		216				1321.0	90.00
4	1 Li^+		215	0.00	0.00	1063.0	3.10
5	1 Li^+	107	107	0.00	0.00	1200.5	46.60
6	1 Li^+	215		0.00	0.00	1321.0	90.00
7	1 BF_4^-		215	0.00	0.00	1063.0	3.10
8	1 BF_4^-	107	107	0.00	0.00	1200.5	46.60
9	1 BF_4^-	215		0.00	0.00	1321.0	90.00
10	1 $LiBF_4$	107	107	0.00	0.00	1200.5	3.10
11	2 $LiBF_4$	126	126	0.0521	0.0446	1174.9	31.42
12	15 $LiBF_4$	46	138	0.9883	0.9101	1178.6	13.04
13	15 $LiBF_4$	92	92	1.0468	0.9153	1241.9	31.42
14	15 $LiBF_4$	140	60	1.0006	0.8459	1276.7	56.56

appeared to be 4.5, whereas the derived Li−O distance was equal to 0.204 nm. The authors suggested that interactions between Li^+ and the F atoms of PF_6^- ion were responsible for the second peak in the data, at around 0.3 nm, whereas the first peak originated due to the Li−O interactions only. We would like to propose that the first peak in the experimental data can also partially characterize the Li−PF_6 interactions, and in particular formation of the $Li^+PF_6^-$ contact ionic pairs (CIP). The assumption about CIP formation should result in a slightly higher RCN value. This interpretation brings the results of ref 17 and our MD simulations into good agreement.

Our MD simulations of infinitely diluted solutions of Li^+ in EC and DMC indicate that the Li^+ FSS in pure solvents consists of 6 molecules. At the same time, the study of Li^+ in the EC−DMC 50%−50% molar mixture shows that the ion's FSS consists of 5 EC molecules and one DMC molecule.

dx.doi.org/10.1021/jp206006m |J. Phys. Chem. B 2011, 115, 14563–14571

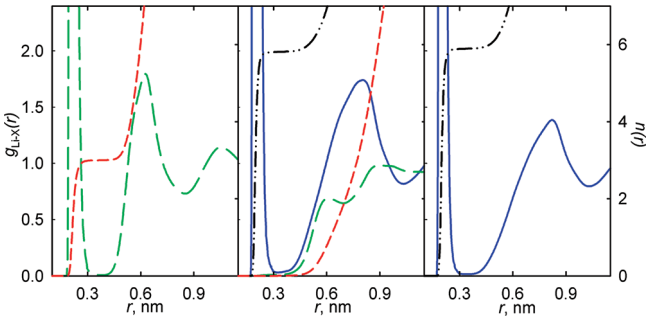

Figure 4. Radial distribution functions $g_{Li\text{-}X}$ (blue solid and green long-dashed) and running coordination numbers $n_{Li\text{-}X}$ (black dash-dotted and red dashed) radial distributions functions for the following systems (Table 3): Li^+−215 DME (left), Li^+−107 PC−107 DME (center), and Li^+−215 PC (right). X stands for $O1_{PC}$ (blue solid and black dash-dotted) and O_{DME} (green long-dashed and red dashed), see Figure 2.

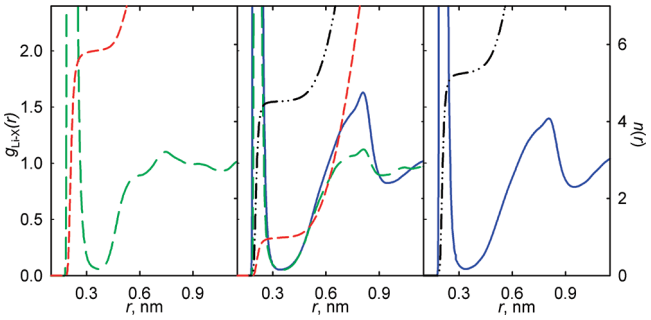

Figure 5. Radial distribution functions $g_{Li\text{-}X}$ (blue solid and green long-dashed) and running coordination numbers $n_{Li\text{-}X}$ (black dash-dotted and red dasherd) radial distributions functions for the following systems (Table 4): Li^+−215 DMC (left), Li^+−107 EC−107 DMC (center), and Li^+−215 EC (right). X stands for $O1_{EC}$ (blue solid and black dash-dotted) and O_{DMC} (green long-dashed and red dashed), see Figure 2.

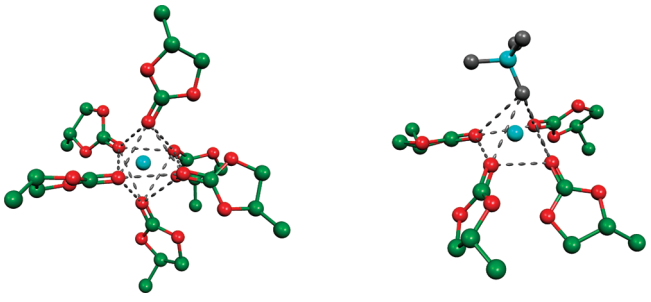

Figure 6. Li^+ first solvation shell for 0.1 M $LiBF_4$ solutions in the 50%−50% PC−DME mixture. See Table 6 for the geometric parameters.

Next, we investigate the structure of the Li^+ FSS for 0.1 M $LiBF_4$ solutions in the PC−DME and EC−DMC mixtures. For this purposes we computed and analyzed the corresponding RDFs and RCNs, and found that the RCN of Li^+ in the PC−DME mixtures is equal to six. In contrast, it is equal to five in the EC−DMC mixtures (Table 5). In PC−DME mixtures, the Li^+ FSS consists of either six PC molecules or five PC molecules and one BF_4^- ion. In the EC−DMC mixtures, the coordination is realized with either five EC molecules or four EC

Table 5. Li^+ FSS Structure for 0.1 M $LiBF_4$ Solutions in the EC−DMC and PC−DME Mixtures

system	interaction centers	r_{max1}, nm	$g_{Li\text{-}X}(r_{max1})$	r_{min1}, nm	$n(r_{min1})$
$2LiBF_4$−106PC−	Li−$O1_{PC}$	0.195	141.3	0.343	5.3
106DME	Li−B	0.327	101.9	0.419	0.3
	Li−F	0.193	105.4	0.261	0.3
$2LiBF_4$−126EC−	Li−$O1_{EC}$	0.203	73.7	0.323	4.0
126DMC	Li−$O1_{DMC}$	0.209	10.3	0.347	0.8
	Li−B	0.327	201.7	0.425	0.5
	Li−F	0.193	199.6	0.261	0.5

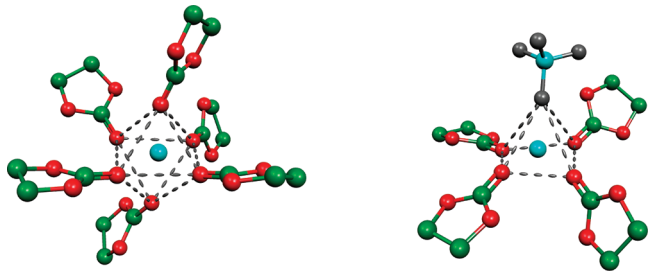

Figure 7. Li^+ first solvation shell for 0.1 M $LiBF_4$ solutions in the 50%−50% EC−DMC mixture. See Table 7 for the geometric parameters.

Table 6. Li^+ FSS Structure in 1.0 M $LiBF_4$ Solutions in the PC−DME Mixtures (Figure 6)

system	interaction centers	r_{max1}, nm	$g_{Li\text{-}X}(r_{max1})$	r_{min1}, nm	$n(r_{min1})$
$16LiBF_4$−43PC−	Li−$O1_{PC}$	0.193	144.7	0.275	2.2
129DME	Li−B	0.415	10.4	0.571	1.6
	Li−F	0.193	104.1	0.257	2.4
$17LiBF_4$−88PC−	Li−$O1_{PC}$	0.195	121.3	0.313	4.3
88DME	Li−B	0.397	2.7	0.553	0.5
	Li−F	0.191	34.5	0.267	0.8
$18LiBF_4$−135PC−	Li−$O1_{PC}$	0.195	91.0	0.329	5.2
45DME	Li−B	0.393	0.9	0.489	0.1
	Li−F	0.189	10.7	0.265	0.3

molecules and one BF_4^- ion coordinated through a fluorine atom (Figures 6 and 7).

At higher concentrations, in particular for 1.0 M $LiBF_4$ in the PC−DME mixtures, we found that the Li^+ RCN is equal to 5 (Table 6). In this case, the FSS structure is determined primarily by interactions between Li^+ and $O1_{PC}$, and to some extent, by interactions of lithium with a fluorine atom of the tetrafluoroborate ion. Interestingly, DME molecules do not participate in the Li^+ FSS in these mixtures.

Switching our attention to the EC−DMC mixtures, we find that the lithium RCN is also equal to 5 (Table 7). However, the FSS is realized through the interactions of the Li^+ ion with the carbonyl oxygen atoms of the EC and DMC molecules, as well as with the fluorine atoms of the tetrafluoroborate ion. The greatest contribution is due to the interactions between Li^+ and BF_4^-, as inferred from the position and height of the first maximum of the RDF (Figure 5), and from the RCN value. The smallest

Table 7. Li^+ FSS Structure in 1.0 M $LiBF_4$ Solutions in the EC−DMC Mixtures (Figure 7)

system	interaction centers	r_{max1}, nm	$g_{Li\text{-}X}(r_{max1})$	r_{min1}, nm	$n(r_{min1})$
$15LiBF_4$−46EC−138DMC	Li−$O1_{EC}$	0.203	65.2	0.309	1.6
	Li−$O1_{DMC}$	0.207	9.4	0.335	0.9
	Li−B	0.325	106.5	0.423	2.6
	Li−F	0.193	103.5	0.265	2.6
$15LiBF_4$−92EC−92DMC	Li−$O1_{EC}$	0.203	38.2	0.311	2.0
	Li−$O1_{DMC}$	0.209	7.3	0.341	0.5
	Li−B	0.325	98.3	0.427	2.6
	Li−F	0.193	95.5	0.261	2.6
$15LiBF_4$−140EC−60DMC	Li−$O1_{EC}$	0.203	34.7	0.323	1.6
	Li−$O1_{DMC}$	0.209	9.2	0.341	0.9
	Li−B	0.325	80.6	0.421	2.0
	Li−F	0.193	78.4	0.265	2.0

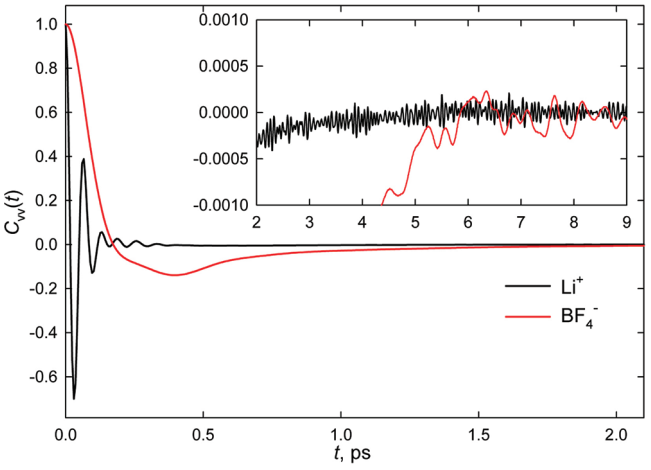

Figure 8. Velocity autocorrelation function $C_{vv}(t)$ for the center-of-mass translational motion of the ions in system 25 (see Table 3).

contribution is made by the interactions of Li^+ with the oxygen atom of the DMC carbonyl group.

It is important to mention here that BF_4^- acts as a bidentate ligand in the PC−DME mixtures, whereas it acts as a monodentate ligand in the EC-DMC mixtures. In particular, the average number of fluorine atoms in the Li^+ FSS exceeds 1.5 in the former case.

4.2. Dynamical Properties. In order to characterize the dynamic properties of the systems in question, the self-diffusion coefficients D_i for the center-of-mass translational motion were calculated using the equation:

$$D_i = \frac{1}{3}\int_0^\infty C_{vv}(t)\,dt \qquad (6)$$

where C_{vv} is the autocorrelation function (ACF) for the linear velocity **v** of the multiatomic particle center-of-mass:

$$C_{vv}(t) = \langle \mathbf{v}(0)\mathbf{v}(t)\rangle \qquad (7)$$

Particular attention was paid to the upper limit of integration of the velocity ACF $C_{vv}(t)$ in the calculation of the D_i values by eq 3. As can be seen in Figure 8, even for the most concentrated and viscous solution (~1 M) of $LiBF_4$ in PC, the ACF of the center-of-mass linear velocity for Li^+ and BF_4^- reaches its zero asymptotic value within the first 6 ps, and at longer time the ACF oscillates around the limit within statistical noise. Thus, 6 ps was chosen as the upper integration limit for the calculation of D_i by eq 6 for all systems under investigation.

Table 8. Dependence of the Diffusion Coefficient on the Fraction of Cyclic Carbonate and Salt Concentration in the PC−DME and EC−DMC Mixtures[a]

c_i, mol·dm^{-3}	$x_{PC\ (EC)}$, %	$D_+\cdot10^9$, m^2·s^{-1}	$D_-\cdot10^9$, m^2·s^{-1}
		PC−DME	
0.0	0	1.22 ± 0.08	2.19 ± 0.10
	25	0.53 ± 0.09	1.12 ± 0.10
	50	0.40 ± 0.01	0.78 ± 0.04
	75	0.27 ± 0.05	0.60 ± 0.06
	100	0.16 ± 0.02	0.46 ± 0.04
0.1	25	0.53 ± 0.04	0.82 ± 0.05
		(0.52 ± 0.03)	(0.83 ± 0.03)
	50	0.31 ± 0.02	0.59 ± 0.08
		(0.31 ± 0.02)	(0.59 ± 0.08)
	75	0.21 ± 0.01	0.38 ± 0.04
		(0.21 ± 0.02)	(0.43 ± 0.03)
	100	0.18 ± 0.02	0.37 ± 0.02
		(0.17 ± 0.01)	(0.39 ± 0.01)
	100	0.22[34]	0.41[34]
1.0	25	0.15 ± 0.02	0.19 ± 0.03
		(0.14 ± 0.01)	(0.14 ± 0.01)
	50	0.10 ± 0.004	0.15 ± 0.01
		(0.098 ± 0.002)	(0.145 ± 0.003
	75	0.09 ± 0.004	0.14 ± 0.01
		(0.086 ± 0.002)	(0.145 ± 0.003)
	100[b]	(0.054 ± 0.003,	(0.113 ± 0.004,
		0.059 ± 0.002)	0.111 ± 0.003)
	100	0.09[34]	0.15[34]
		EC−DMC	
0.0	0	0.62 ± 0.06	1.64 ± 0.16
	50	0.55 ± 0.07	1.06 ± 0.05
	100	0.36 ± 0.04	0.84 ± 0.12
0.1	50	0.57 ± 0.07	0.95 ± 0.08
1.0	25	0.23 ± 0.02	0.24 ± 0.03
	50	0.19 ± 0.02	0.20 ± 0.02
	70	0.22 ± 0.01	0.27 ± 0.03

[a] The values in parentheses correspond to the longer simulations indicated in Table 3. [b] For systems 24 and 25, respectively; see Table 3.

The diffusion coefficients were calculated for the infinitely diluted, 0.1 and 1.0 M solutions (Table 8). A good overall agreement is seen between the calculated and experimental[34] diffusion coefficients of the Li^+ and BF_4^- ions in pure PC. The agreement is best for the 0.1 M solution.

In the concentrated solutions of $LiBF_4$ in the PC−DME and EC−DMC mixtures, the diffusion coefficients of both cation (D_+) and anion (D_-) decreased with increasing fraction of the cyclic component (PC and EC, Figure 1). This is due to the growth of the viscosity of the solvent mixture. The small increase in the ions' D_i values in the EC−DMC mixture at the EC molar fraction of 70% is caused by partial destruction of the $Li^+BF_4^-$

Table 9. Limiting Molar Conductivity of Infinitely Diluted Li^+ Solutions in the PC−DME Mixtures

x_{PC}, %	25	50	75	100
R_i^s, nm	0.7898	0.7898	0.7898	0.8365
η (MD), mPa·s	0.60 ± 0.12	1.02 ± 0.06	1.5 ± 0.3	2.9 ± 0.4
$\lambda_i^0(D_i)$, S·cm^2·mol^{-1}	19 ± 1	12 ± 3	8 ± 1	6 ± 1
$\lambda_i^0(R_i^s)$, S·cm^2·mol^{-1}	25 ± 4	15 ± 1	10 ± 2	5
λ_i^0 (exp), S·cm^2·mol^{-1}				7.18[34], 7.30[35]

CIP. This explanation is supported by the decreased Li^+−B and Li^+−F RCNs, which indicate weakening of the Li^+−BF_4^- interaction. Further, our MD simulations showed that ion diffusion coefficients were significantly lower in the PC−DME mixtures than in the EC−DMC mixtures, most likely due to the difference in the viscosities of these systems.

The Stokes' model provides the simplest description of ion dynamics in solution. Generally, the Stokes' description is applicable to relatively large ions, while Li^+ is very small. However, assuming that Li^+ moves along with its solvation shell, one can expect the Stokes' model to provide adequate results for the current systems as well.

In order to test the applicability of the Stokes' model to the Li^+ ion systems investigated in the present paper, the limiting values of molar conductivity λ_i^0 were calculated for the infinitely diluted Li^+ solutions in the PC−DME mixtures. The calculations were carried out in two independent ways: first, based on the D_i values, and second, using the effective radius of the Li^+ FSS, R_i^s. The effective radius was computed as the sum of the position of the first minima of the Li-CH_3 RDF with $1/2\sigma_{ii}$ for the CH_3 group (Table 9). In particular, the following two formulas were used:

$$\lambda_i^0 = \frac{z_i^2 F^2}{RT} D_i \tag{8}$$

$$\lambda_i^0 = \frac{z_i e F}{4\pi\eta R_i^s} \tag{9}$$

where z_i is ion's charge.

As seen from Table 9, the limiting molar conductivity values are consistent between the two methods, and the theoretical results agree with the data of conductometric experiments[35,36] for pure PC. The calculated λ_i^0 values show the same trend, decreasing with an increase of the PC fraction, due to growth of the systems' viscosity. These calculations indicate that stability of the FSS in these and similar systems allows one to apply the Stokes' model in order to obtain an estimate of molar conductivity.

5. CONCLUSIONS

We developed reliable force-field models of the ethylene carbonate, propylene carbonate, dimethyl carbonate and dimethoxyethane solvent molecules using the results of quantum chemical calculations. The models successfully account for the experimental macroscopic properties of these solvents, including heat of vaporization, viscosity, and dielectric permittivity.

We used the developed models to carry out detailed MD simulations on a broad range of systems including pure EC, PC, DMC and DME; PC−DME and EC−DMC mixtures with a variety of compositions; infinitely diluted Li^+ and BF_4^- solutions in pure solvents and their mixtures; $Li^+BF_4^-$ ion pair in DME and $LiBF_4$ in EC−DMC; and $LiBF_4$ solutions with concentrations of approximately 0.1 and 1.0 mol·dm^{-3} in PC, PC−DME and EC−DMC. A number of important and sometimes surprising results were obtained.

The MD simulations showed that an increase of the salt concentration results in a decrease of the cation coordination number from 6, for infinitely dilute solutions, to 5, for 1.0 M solutions. The interaction between the Li^+ ion and solvent molecules proceeds primarily via the oxygen atoms of the solvent. Moreover, the carbonyl oxygens play a significantly more important role than the oxygens inside the hydrocarbon chain, due to a larger negative charge on the carbonyl oxygens.

Surprisingly at first, the lithium ion is solvated in mixed solvents preferentially by cyclic molecules, even though they possess less conformational flexibility, and therefore a priori, may be expected to generate larger steric hindrances. In the case of infinitely diluted and 0.1 M solutions of $LiBF_4$, the lithium ion is coordinated by 6 PC molecules in the PC−DME mixtures, and by 5 EC molecules and one DMC molecule in the EC−DMC mixtures. Such large asymmetry in the PC−DME mixture is rationalized by the absence of a carbonyl group, and the general lack of strong negative atomic charges in the DMC molecule. Even though both EC and DMC molecules contain carbonyls, the asymmetry in the solvation structure is significant in the EC−DMC mixture as well. From the practical point of view, one can take advantage of the solvation asymmetry and vary individual solvent components and mixture composition in order to reduce electrolyte viscosity, while maintaining its high electrical conductivity.

At high salt concentrations, Li^+ is solvated by a combination of cyclic carbonates and counterions, and contact ion pairs are formed. The BF_4^- anion acts as a monodentate ligand in the PC−DME mixtures and a bidentate ligand in the EC−DMC mixtures. In 1.0 M solutions of $LiBF_4$, the cation and anion diffusion coefficients decrease with increasing fraction of the cyclic carbonate. True for both mixtures, this is due to the growth of mixture viscosity. Interestingly, the trend is disrupted at certain EC−DMC compositions because of the solvent induced weakening of the electrostatic interaction in the Li^+ BF_4^- ion pair. A similar enhancement of ionic conductivity as a result of disruption of the potential around the Li^+ ion was observed in polymer electrolytes.[37]

Notably, the Stokes model of diffusion applies to the Li^+ ion, even though the ion is very small, while the Stokes' description is expected to apply only to relatively large ions. The model works, because the Li^+ ion creates a strongly bound solvation shell, and the size of the shell rather than that of the ion alone should be used in the calculation. This result shows that the Stokes diffusion model can be used to obtain estimates of conductivities of solutions involving small ions.

The results reported in the study are important for understanding of the operation of modern lithium-ion batteries. They provide molecular level principles for the optimization of electrolyte properties, such as electrical conductivity and viscosity.

AUTHOR INFORMATION

Corresponding Author

*E-mail: oleg.prezhdo@rochester.edu.

ACKNOWLEDGMENT

The research was supported in part by the NSF Grant CHE-1050405.

REFERENCES

(1) Xu, K. *Chem. Rev.* **2004**, *104*, 4303–4417.
(2) Armand, M.; Grugeon, S.; Vezin, H.; Laruelle, S.; Ribiere, P.; Poizot, P.; Tarascon, J. M. *Nat. Mater.* **2009**, *8*, 120–125.
(3) McCloskey, B. D.; Bethune, D. S.; Shelby, R. M.; Girishkumar, G.; Luntz, A. C. *J. Phys. Chem. Lett.* **2011**, *2*, 1161–1166.
(4) Zhang, Y. C.; Alonso, P. R.; Martinez-Limia, A.; Scanlon, L. G.; Balbuena, P. B. *J. Phys. Chem. B* **2004**, *108*, 4659–4668.
(5) McDonagh, P. M.; Reardon, J. F. *J. Solution Chem.* **1996**, *25*, 607–614.
(6) Reardon, J. F. *Electrochim. Acta* **1987**, *32*, 1595–1600.
(7) Yang, Z.; Wang, J.; Tang, J.; Zhuo, K. *J. Mol. Liq.* **2006**, *128*, 65–70.
(8) Masia, M.; Rey, R. *J. Phys. Chem. B* **2004**, *108*, 17992–18002.
(9) Borodin, O.; Smith, G. D. *J. Phys. Chem. B* **2006**, *110*, 6293–6299.
(10) Vorobyov, I.; Anisimov, V. M.; Greene, S.; Venable, R. M.; Moser, A.; Pastor, R. W.; MacKerell, A. D. *J. Chem. Theory Comput.* **2007**, *3*, 1120–1133.
(11) Borodin, O.; Smith, G. D. *J. Phys. Chem. B* **2006**, *110*, 6279–6292.
(12) Hayamizu, K.; Aihara, Y.; Nakagawa, H.; Nukuda, T.; Price, W. S. *J. Phys. Chem. B* **2004**, *108*, 19527–19532.
(13) Nakade, S.; Kambe, S.; Kitamura, T.; Wada, Y.; Yanagida, S. *J. Phys. Chem. B* **2001**, *105*, 9150–9152.
(14) Fraenkel, D. *J. Phys. Chem. B* **2011**, *115*, 557–568.
(15) Tarascon, J. M.; Armand, M. *Nature* **2001**, *414*, 359–367.
(16) Xu, K. *Chem. Rev.* **2004**, *104*, 4303–4417.
(17) Kameda, Y.; Umebayashi, Y.; Takeuchi, M.; Wahab, M. A.; Fukuda, S.; Ishiguro, S.-i.; Sasaki, M.; Amo, Y.; Usuki, T. *J. Phys. Chem. B* **2007**, *111*, 6104–6109.
(18) Jeager, H. L.; Fedyk, J. D.; Parker, R. J. *J. Phys. Chem.* **1973**, *77*, 2407–2410.
(19) Barthel, J.; Buchner, R.; Wismeth, E. *J. Solution Chem.* **2000**, *29*, 937–954.
(20) Henderson, W. A.; Brooks, N. R.; Brennessel, W. W.; Young, V. G. *J. Phys. Chem. A* **2003**, *108*, 225–229.
(21) Salomon, M.; Plichta, E. J. *Electrochim. Acta* **1985**, *30*, 113–119.
(22) Soetens, J.-C.; Millot, C.; Maigret, B. *J. Phys. Chem. A* **1998**, *102*, 1055–1061.
(23) Soetens, J.-C.; Millot, C.; Maigret, B.; BakÛ, I. *J. Mol. Liq.* **2001**, *92*, 201–216.
(24) Allen, M. P., T. D. J. *Computer simulation of liquids*; Clarendon press: Oxford, 1987.
(25) Frisch, M. J.; Trucks, G. W.; Schlegel, H. B.; Scuseria, G. E.; Robb, M. A.; Cheeseman, J. R.; Montgomery, J. A.; Vreven, T.; Kudin, K. N.; Burant, J. C. et al. Gaussian 03, Revision B.01, 2003.
(26) Breneman, C. M.; Wiberg, K. B. *J. Comput. Chem.* **1990**, *11*, 361–373.
(27) van Gunsteren, W. F.; Billeter, S. R.; Eising, A. A.; Hunenberger, P. H.; Kruger, P.; Mark, A. E.; Scott, W. R. P.; Tironi, I. G. *Biomolecular Simulation: The {GROMOS96} manual and userguide*; Hochschuleverlag AG an der ETH: Zurich, 1996.
(28) Peng, Z.; Ewig, C. S.; Hwang, M.-J.; Waldman, M.; Hagler, A. T. *J. Phys. Chem. A* **1997**, *101*, 7243–7252.
(29) Marcus, Y. *The properties of solvents*: John Wiley and Sons Ltd.: Chechester, U.K., 1998; Vol. 4.
(30) Barthel, J.; Neueder, R.; Roch, H. *J. Chem. Eng. Data* **2000**, *45*, 1007–1011.
(31) Naejus, R.; Lemordant, D.; Coudert, R.; Willmann, P. *J. Chem. Thermodyn.* **1997**, *29*, 1503–1515.
(32) Kalugin, O. N.; Volobuev, M. N.; Kolesnik, Y. V. *Kharkov Univ. Bull., Chem. Ser.* **1999**, *4*, 58.
(33) Annapureddy, H. V. R.; Kashyap, H. K.; De Biase, P. M.; Margulis, C. J. *J. Phys. Chem. B* **2010**, *114*, 16838–16846.
(34) Takeuchi, M.; Kameda, Y.; Umebayashi, Y.; Ogawa, S.; Sonoda, T.; Ishiguro, S. I.; Fujita, M.; Sano, M. *J. Mol. Liq.* **2009**, *148*, 99–108.
(35) Salomon, M.; Plichta, E. *Electrochim. Acta* **1983**, *28*, 1681–1686.
(36) Mukherjee, L. M.; Boden, D. P.; Lindauer, R. *J. Phys. Chem.* **1970**, *74*, 1942.
(37) Christie, A. M.; Lilley, S. J.; Staunton, E.; Andreev, Y. G.; Bruce, P. G. *Nature* **2005**, *433*, 50–53.